Band-gap state engineering in rutile TiO_2 (110) surface by modulating the active heteroatom

Yaoguang Yu, Xu Yang, Yanling Zhao,* Xiangbin Zhang, Liang An, Miaoyan Huang, Gang Chen and Ruiqin Zhang*

Abstract: Introducing band-gap states to TiO_2 photocatalyst is an efficient strategy for expanding the utilization of solar spectrum. However, few approaches are capable of introducing band-gap states and improving the photocatalytic performance, simultaneously. Especially toward the reactions requiring unambiguous adsorption sites as the prerequisite, introducing band-gap states by creating surface disorder is incapacitated. Herein, we show the feasibility of introducing band-gap states via an alternative approach in which the selected heteroatom is implanted to the preferred surface sites. The theoretical prediction and the subsequent experimental verification reveal that the implanted heteroatoms not only introduce band-gap states without resorting to the surface disorder but act as active sites for Cr(VI) reduction reaction. This work represents a potent approach to introduce band-gap states and may open an encouraging start in designing highly efficient surface for solar harvesting materials.

Attributed to its enthralling features such as low cost, inertness, nontoxicity, TiO_2 is regarded as one of the most promising functional materials in environmental and energy fields.[1] In order to take a quantum leap in performance, immense efforts have been devoted to design and synthesize advanced TiO_2 photocatalyst, whereas narrowing the band gap to harvest solar energy is the prerequisite. Nonmetal incorporation such as N,[2] S[3] and I[4] has been widely used to modulate the electronic structures thus extending the light absorption. However, extended light absorption does not always signify an enhanced performance since a highly efficient charge separation also plays a crucial role. The band tail state, which is one type of band-gap states, can not only narrow the band gap but inhibit the spatial recombination of itinerant electrons by localizing the photo-induced holes.[5] Introducing band-gap states to the surface electronic structure of TiO_2 photocatalyst is thus a trendsetting strategy to achieve the wide solar spectral response and efficient photo-induced charge separation. Up to date, only the creation of surface disorder is widely accepted as an effective approach to introduce the band tail state, which is manifested by the pronounced solar water splitting performance in hydrogenated TiO_2.[6] The broken surface Ti-O bonds in hydrogenated TiO_2 are saturated by H atoms leaving Ti-H and O-H bonds terminated highly disordered surface atomic arrangement. The consequent band tail states thus expedite the solar water splitting reaction.[7]

Note that the surface region of photocatalysts not only functions as the collector of photo-induced charge carriers but regulates the selectivity of designated reaction by the interaction with reactants.[8] Toward prodigious photocatalytic reactions that slow adsorption kinetics restrains the overall reaction rate, the surface providing unambiguous adsorption sites is more favorable. For instance, the photocatalytic reduction of chromate (VI) ions on the surface of rutile TiO_2 (110) in acidic condition is initialized by the adsorption of chromate (VI) ions on Ti_{5C} (5-fold coordinated Ti atoms) and protonated O_{2C} sites synchronously through chemical bond and hydrogen bond.[9] In other words, tailored surface is more essential for the photocatalytic reduction of chromate (VI) ions compared with the disordered surface.

Indeed, an efficient photocatalyst conductive to the transformation of pollutant molecules should fulfill three requirements simultaneously: i) narrow band gap for solar energy harvesting; ii) efficient separation of photo-induced charges and subsequent precise delivery of charge carriers to promote the photocatalytic performance; and iii) exquisitely designed arrangement of surface atom to capture reactants expeditiously. Herein, we present a well-designed N-modified (110) surface of rutile TiO_2. The in-plane O_{3C} selectively substituted by N_{3C} matches our prediction based on the theoretical calculation, which introduces the band-gap state without resorting to the surface disorder. Attributed to the expansion of light absorption range, efficient separation of charge carriers and quick surface process delivered by the present approach, the N-modified rutile (110) surface exhibits remarkable performance for Cr(VI) reduction among TiO_2 photocatalysts.

The most possible location of N dopant on the surface of rutile TiO_2 (110) is firstly evaluated by the minimum of the surface energy as conducted by DFT calculations. Since the substitution of N for Ti is energetically unfavorable[10] and interstitial doping usually pays a higher kinetic price than the substitutional mode,[11] the remaining substitutional modes of N for O_{3C} (in-plane O) and O_{2C} (bridge-bonded oxygen, BBO) are investigated in this case (Fig. 1a). The surface energy of substitutional doping N for O_{3C} (0.54 $J \cdot m^{-2}$) is comparable with the unmodified surface (0.48 $J \cdot m^{-2}$), whereas drastically

Dr. Y. G. Yu, X. Yang, X. B. Zhang, Prof. G. Chen
MIIT Key Laboratory of Critical Materials Technology for New Energy Conversion and Storage, School of Chemistry and Chemical Engineering, Harbin Institute of Technology, Harbin, P. R. China

[*] Dr. Y. G. Yu, Dr Y. L. Zhao, M. Y. Huang, Prof R. Q. Zhang
Department of Physics, City University of Hong Kong, Hong Kong SAR, P. R. China
E-mail: apzyl@cityu.edu.hk

Dr. L. An
Department of Mechanical Engineering, The Hong Kong Polytechnic University, Hong Kong SAR, P. R. China

Prof R. Q. Zhang
Shenzhen Research Institute, City University of Hong Kong, Shenzhen, P. R. China
E-mail: aprqz@cityu.edu.hk

Supporting information for this article is given via a link at the end of the document.

increased surface energy of substitutional doping N for O_{2C} (0.81 J·m^{-2}) is observed. This indicates the substitution of N for O_{3C} is thermodynamically more favorable. To further explore the contribution of in-plane N dopant to the surface electronic structure, the difference of the surface PDOS between in-plane N doping and unmodified surface of rutile TiO_2 (110) is analyzed (Fig 1b). The conduction band minima (CBM) of both surfaces are dominantly composed of the 3d orbitals of Ti_{5C} atoms. The wide distribution of the Ti_{5C}-3d CBM states indicates that the photo-induced electrons are endowed with itinerant feature. In contrast, the in-plane N doping converts the composition of valence band maximum (VBM) from the mixture of the 2p orbitals of O_{2C} and O_{3C} atoms to dominant 2p orbital of N_{3C} atoms. The strongly localized 2p orbitals of N_{3C} atoms penetrated by the Fermi level separate band-gap states into two parts: i) states below the Fermi level localized the hole to prevent the recombination; and ii) states above the Fermi level provided unoccupied orbitals for photo-induced electrons to facilitate the VB to CB transition. Consequently, selectively substitutional doping N for in-plane O will not only maintain the surface structure of pristine rutile TiO_2 (110) but provide band-gap states to promote the charge separation.

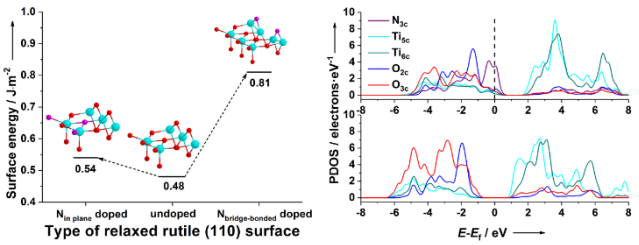

Fig 1 a) Surface energies of unmodified (middle), substitutional doping N for O_{3C} (left) and substitutional doping N for O_{2C} (right) models. b) Surface PDOS of unmodified rutile (110) (lower) and substitutional doping N for O_{3C} surface (upper). The surface N atom in a three-coordination environment is denoted as N_{3C} and the other atoms are abbreviated by analogy.

Although the theoretical prediction suggests a satisfying surface energy and a promising surface electronic structure, the O_{3C} atom bonded with one more Ti atom compared with O_{2C} atom leads a higher kinetic barrier to achieve substitutional doping. By means of weakening the Ti-O bond, three serial treatments were employed to accomplish this goal (Fig. S1). The rutile TiO_2 with trace residuals was firstly synthetized via hydrothermal hydrolysis of TiB_2 at the pH value of 0.55. The subsequent calcination treatment at 600 °C removed the residuals and drove the B atoms to the surface interstitial sites of the rutile TiO_2, simultaneously.[12] After the final surface nitridation, the N dopant can substitute for the O_{3C} atom attributed to the weakened surface Ti-O bond by interstitial B atoms.[2] The final product displays the nanorod shape with 1-2 μm in length and 100-200 nm in diameter (Fig. 2a). The nanorods are enclosed by well-defined facets (Fig. S2). The SAED pattern acquired along the [110] zone axis confirms the single-crystalline nature of the nanorod (Fig. 2b). The interplanar spacings of 0.32 nm and 0.29 nm with the angle of 90° are the same as the spacing of {110} and {001} planes and the corresponding intersection angle in rutile TiO_2, which indicates the rutile nanorods are predominantly enclosed by (110) facets (Fig. 2c). To confirm the implantation of N atoms, XEDS-mapping is carried out on the terminal of a randomly selected nanorod (Fig. 2d). The XEDS-mapping images reveal that Ti, O and N elements are homogeneously distributed, and no noticeable compositional distribution is detected throughout the test region. This result verifies the successful implantation of N atoms into the surface of rutile TiO_2. It is worth noting that the acquired signal of B element does not match the profile of the HAADF image, indicating the completely removal of B element from the surface (Fig. S3). Consequently, N atoms are successfully implanted into the surface region of rutile TiO_2 nanorods enclosed predominantly by (110) facets.

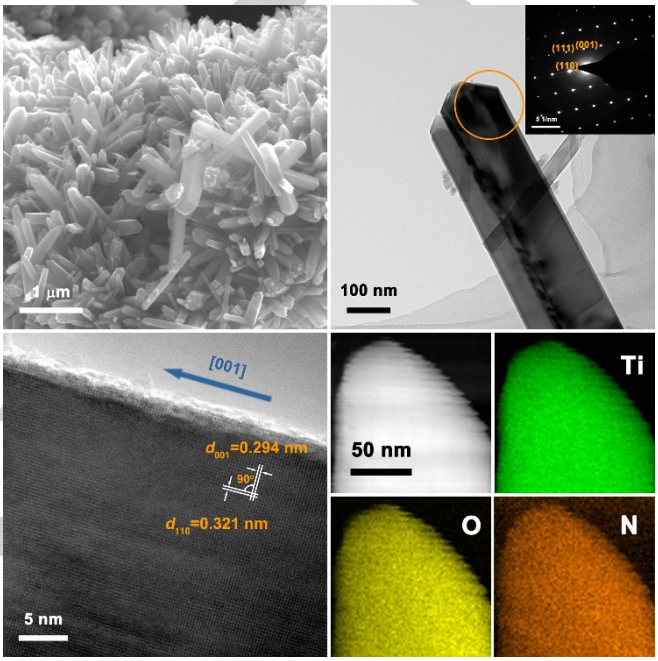

Fig. 2 Electron microscopy characterization of the N-TiO_2: a) FESEM image, b) TEM image, c) HRTEM image and d) XEDS-mapping images. The inset in TEM image is the SAED pattern acquired from the marked region.

In order to validate the location of N atoms on rutile (110) surface, XPS analysis is introduced to investigate the chemical status of surface Ti, O and N atoms. On the rutile (110) surface, two types of Ti atoms (Ti_{6C} and Ti_{5C} atoms) can be identified. However, the binding energies of Ti 2p core levels at 465.2 eV and 459.1 eV assigned to the photoelectrons from Ti $2p_{1/2}$ and Ti $2p_{3/2}$ spin-orbital splitting correspond to the Ti^{4+} chemical state[13] (Fig. 3a). No signal assigned to Ti^{3+} or other Ti species is observed, which confirms the sole Ti^{4+} species on the rutile (110) surface. On the other hand, two types of O atoms (O_{3C} and O_{2C} atoms) can be identified on the ideal surface of rutile (110). The O_{3C} atoms are evidenced by the binding energy of O 1s core level at 529.4 eV[14] (Fig. 3b). As for the case of O_{2C} atoms, a Ti_{6C} atom is surrounded by one N_{3C}, two O_{2C} and three O_{3C} atoms to form a $Ti_{6C}(O_{3C})_3(O_{2C})_2N_{3C}$ octahedron (Fig. 3d) remaining one valence electron in excess. Accordingly, the excess valence electron in O_{2C} atom can bond with H^+ to form hydrogenated O_{2C}, which is evidenced by the binding energy of O 1s core level at 531.2 eV[15] (Fig. 3b). Similar to the condition of Ti atoms, the binding energy of N 1s core level at 396.6 eV also demonstrates the sole chemical environment of surface N atoms, which is usually regarded as the substitution of N for O.[16] It is worth mentioning that the traditional substitution of N for O is usually stabilized by oxygen vacancies due to

requirement of charge neutrality, thus leading to Ti^{3+} as the recombination center.[17] In the present work, we provide an alternative strategy to achieve the substitution of N for O without resorting to oxygen vacancies, much less the Ti^{3+} species.

Notwithstanding multitudinous novel photocatalysts, Degussa P25, a commercially available mixture of anatase, rutile and amorphous TiO_2, is still a benchmark photocatalyst for evaluating the photocatalytic performance.[18] To further explore the optical and photocatalytic property of N-modified rutile TiO_2 (N-TiO_2), N doped P25 (N-P25) synthetized via the same nitriding condition is selected as the benchmark. Besides, the UV-vis spectrum of white TiO_2 calcined in the air (rutile TiO_2, Fig. S1) is also recorded for a fair comparison. Both white TiO_2 and N-TiO_2 exhibit steep absorption edges with the band gap energy of 3.10 and 2.95 eV, respectively (Fig. 4a, S4 and Table S1). For N-P25, two disparate absorption edges corresponding to the band gap energy of 3.01 eV and 3.14 eV are observed, which can be assigned to N doped rutile and anatase, respectively. Compared with the white TiO_2, both N-TiO_2 and N-P25 exhibit bathochromic shift and enhanced absorption beyond their absorption edges even if the absorption may not contribute to the photocatalytic reaction. This phenomenon matches well with the DFT prediction (Fig. S4) that the absorption edge of N-TiO_2 is ascribed to the excitation from the band-gap states above the Fermi level to the CBM, while the absorption beyond the absorption edge is ascribed to the excitation to the band-gap states above the Fermi level from the lower energy states. By shortening half of the nitridation time, the absorption edge of the control sample exhibits hypsochromic shift and reduced absorption beyond the absorption edge in comparison with N-TiO_2 (Fig. S5). However, the identical band gaps of the control sample (3.00 eV) and N doped rutile in N-P25 (3.01 eV) suggest the improved nitrogen solubility in the surface region of N-TiO_2, which is also evidenced by the XPS elemental composition analysis (Table S1).

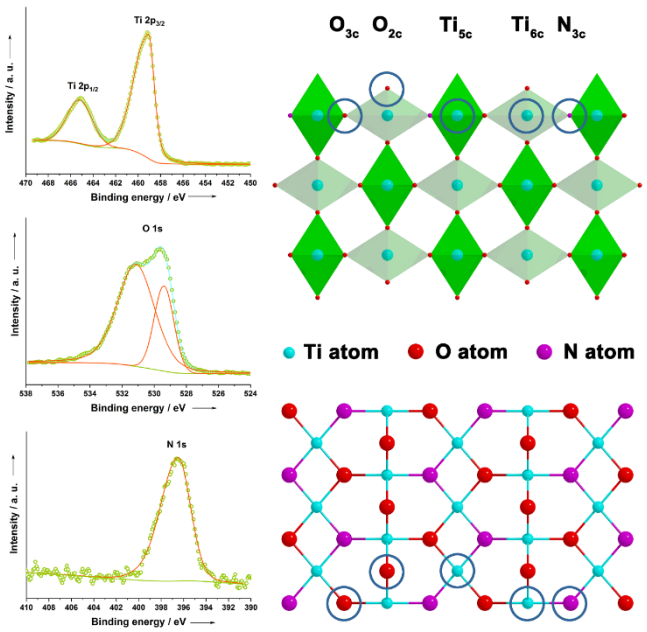

Fig. 3 XPS spectra of N-TiO_2: a) Ti 2p, b) O 1s, c) N 1s core levels and d) the surface atomic arrangement of N-TiO_2 viewing along [001] (upper) and [110] (lower) direction.

Due to the fact that the substitutional doping N for O_{2C} will result in oxygen vacancy associated with Ti^{3+}, EPR technique is utilized to further assess the location of N dopant between O_{3C} and O_{2C} sites (Fig. 4b). The EPR signal for g-value of 2.005 is observed both in N-TiO_2 and N-P25. This value is quite close to the previously reported g-value of 2.007 for Ti^{4+}-O^{2-}-Ti^{4+}-$O^{\bullet-}$ radical, which is a characteristic signal in pristine TiO_2.[19] Besides, the g-value of 1.990 for N-P25 can be assigned to one electron trapped in anatase TiO_2, whereas the g-value of 1.969 and 1.947 can be ascribed to more than one type of Ti^{3+} species in N-P25.[20] The EPR results provide two solid evidences: i) substitutional doping N for O_{3C} maintains the rhombic oxygen ligand field without involving additional paramagnetic center; and ii) the precursor is crucial to achieve the substitutional doping N for O_{3C}, otherwise oxygen vacancies and Ti^{3+} species will be involved.

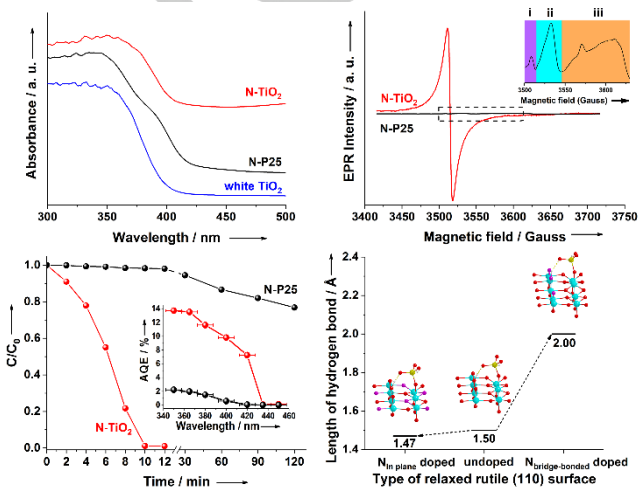

Fig. 4 a) UV-vis absorption spectra of white TiO_2, N-P25 and N-TiO_2. b) EPR spectra of N-P25 and N-TiO_2. The inset is the magnified view of the EPR spectrum for N-P25. The EPR signals in region i, ii and iii correspond to the g-values of 2.005, 1.990, 1.969 and 1.947, respectively. c) Photocatalytic Cr(VI) reduction over N-TiO_2 and N-P25 in the presence of citrate tri-anions under AM1.5G illumination. The inset is the action spectra. d) Length of hydrogen bond between $HCrO_4^-$ and surface of unmodified (middle), substitutional doping N for O_{3C} (left) and substitutional doping N for O_{2C} (right).

The photocatalytic performance of N-TiO_2 is evaluated through Cr(VI) reduction along with citric acid. In acidic condition, $HCrO_4^-$ ion is the dominant species of chromate ions.[21] The tailored rutile (110) facet associated with substitutional doping N for the O_{3C} can provide unambiguous Ti_{5C} and hydrogenated O_{2C} sites for the adsorption of $HCrO_4^-$. Moreover, the separate sites for adsorption process and oxidative reaction (O_{2C} and N_{3C} sites, respectively) will avoid the steric effect on pristine surface that both the $HCrO_4^-$ ion and the citric acid molecule compete for the O_{2C} site. The performance test also emphasizes the outstanding capacity of N-TiO_2 for Cr(VI) reduction (Fig. 4c, Table S3). In contrast, less than 25% of chromate (VI) ions are reduced over N-P25 under the same experimental condition even with prolonged irradiation time by one order of magnitude. Noting that the specific surface area of N-P25 (47 $m^2 \cdot g^{-1}$) is larger than that of N-TiO_2 (35 $m^2 \cdot g^{-1}$), which further emphasizes the active surface of N-TiO_2 (Fig. S6 and Table S1). The profiles of the action spectra match well with the UV-Vis absorption spectra for N-TiO_2 and N-P25, which further proves that the

activities of Cr(VI) reduction over N-TiO_2 and N-P25 originate from electrons excited from VB to CB transition. In addition, the apparent quantum efficiency at 400 nm still reached 9.8% for N-TiO_2 compared with ca. 0.6% for N-P25, which holds tremendous potential in the practical application of photocatalytic Cr(VI) removal from sewage. Moreover, the significantly discrepant capacity in photo-induced charge separation between N-TiO_2 and N-P25 accentuates the ascendancy of substitutional doping N for O_{3C} on rutile (110) surface (Fig. S7).

It is reported that the hydrogen bond induced adsorption greatly enhances the electron transfer between H–O_{BBO} on TiO_2 surface and adsorbates.[22] Similar effect of enhanced charge transfer induced by hydrogen bond is also found in the graphitized carbon nitride (g-CN) system.[23] Accordingly, the lengths of hydrogen bond of $HCrO_4^-$ adsorbed on unmodified, substitutional doping N for O_{3C} and substitutional doping N for O_{2C} rutile (110) surface models are calculated, respectively (Fig. 4d). Compared with the length of hydrogen bond (1.47 Å) in substitutional doping N for O_{3C} model, the length of hydrogen bond (2.00 Å) in substitutional doping N for O_{2C} model is exceedingly expanded, which further emphasizes the enhanced charge transfer between the modified rutile (110) surface and $HCrO_4^-$. In addition, the enhanced charge transfer is also validated through RhB degradation reaction (Fig. S8).

In summary, we have shown the feasibility of introducing band-gap states by implanting selected heteroatoms to the preferred surface sites. The selectively substitutional doping N for in-plane O maintains the surface structure of rutile TiO_2 (110), and further provides band-gap states above the Fermi level to promote the charge separation and migration. Attributed to the unambiguous adsorption sites and efficient surface charge transfer of N-modified rutile TiO_2 (110), over 15-fold enhancement of apparent quantum efficiency at 400 nm is achieved compared with N doped Degussa P25. This finding may broaden the way of TiO_2-based materials in environmental application and provide insight into the principle of band-gap engineering for the design of solar harvesting catalysts.

Acknowledgements

This work was financially supported by the National Natural Science Foundation of China (21601042), China Postdoctoral Science Foundation funded project (2015M571410), Guangdong-Hong Kong Technology Cooperation Funding Scheme (2017A050506048) and Science Technology and Innovation Committee of Shenzhen Municipality (JCYJ20160229165210666). Y. G. Yu thank the support from the " Hong Kong Scholars Program". Y. G. Yu thank Dr. Steve Kershaw for the PL characterization and the helpful discussion.

Keywords: photocatalysis • band-gap state • density functional theory • rutile TiO_2 • Cr(VI) reduction

[1] L. Liu, X. Chen, *Chem. Rev.* **2014**, 114, 9890-9918.
[2] G. Liu, L. C. Yin, J. Wang, P. Niu, C. Zhen, Y. Xie, H. M. Cheng, *Energy Environ. Sci.* **2012**, 5, 9603- 9610.
[3] C. Y. Yang, Z. Wang, T. Q. Lin, H. Yin, X. J. Lü, D. Y. Wan, T. Xu, C. Zheng, J. H. Lin, F. Q. Huang, X. M. Xie, M. H. Jiang, *J. Am. Chem. Soc.* **2013**, 135, 17831–17838.
[4] T. Q. Lin, C. Y. Yang, Z. Wang, H. Yin, X. J. Lü, F. Q. Huang, J. H. Lin, X. M. Xie, M. H. Jiang, *Energy Environ. Sci.* **2014**, 7, 967-972.
[5] L. Liu, P. Y. Yu, X. Chen, S. S. Mao, D. Z. Shen, *Phys. Rev. Lett.* **2013**, 111, 065505.
[6] X. Chen, L. Liu, F. Huang, *Chem. Soc. Rev.* **2015**, 44, 1861-1885.
[7] X. Chen, L. Liu, P. Y. Yu, S. S. Mao, *Science* **2011**, 331, 746-750.
[8] a) J. Zhang, Q. Xu, Z. Feng, M. Li, C. Li, *Angew. Chem. Int. Ed.* **2008**, 47, 1766-1769; b) S. Bai, L. Wang, Z. Li, Y. Xiong, *Adv. Sci.* **2017**, 4, 1600216.
[9] G. Zou, J. Guo, Q. Peng, A. Zhou, Q. Zhang, B. Liu, *J. Mater. Chem. A* **2016**, 4, 489-499.
[10] S. Hoang, S. P. Berglund, N. T. Hahn, A. J. Bard, C. B. Mullins, *J. Am. Chem. Soc.* **2012**, 134, 3659-3662.
[11] M. Ceotto, L. Lo Presti, G. Cappelletti, D. Meroni, F. Spadavecchia, R. Zecca, M. Leoni, P. Scardi, C. L. Bianchi, S. Ardizzone, *J. Phys. Chem. C* **2012**, 116, 1764-1771.
[12] G. Liu, J. Pan, L. Yin, J. T. S. Irvine, F. Li, J. Tan, P. Wormald, H. M. Cheng, *Adv. Funct. Mater.* **2012**, 22, 3233-3238.
[13] H. Zhang, P. Xu, G. Du, Z. Chen, K. Oh, D. Pan, Z. Jiao, *Nano Research* **2010**, 4, 274-283.
[14] a) Y. Y. Song, Z. D. Gao, J. H. Wang, X. H. Xia, R. Lynch, *Adv. Funct. Mater.* **2011**, 21, 1941-1946; b) Y. Wang, L. Zhang, S. Li, P. Jena, *J. Phys. Chem. C* **2009**, 113, 9210-9217.
[15] a) H. K. Seo, C. M. Elliott, H. S. Shin, *ACS Appl. Mater. Interfaces* **2010**, 2, 3397-3400; b) S. K. Kim, G. J. Choi, S. Y. Lee, M. Seo, S. W. Lee, J. H. Han, H. S. Ahn, S. Han, C. S. Hwang, *Adv. Mater.* **2008**, 20, 1429-1435.
[16] a) J. B. Varley, A. Janotti, C. G. Van de Walle, *Adv. Mater.* **2011**, 23, 2343-2347; b) T. Ohsawa, I. Lyubinetsky, Y. Du, M. A. Henderson, V. Shutthanandan, S. A. Chambers, *Phys. Rev. B* **2009**, 79, 085401.
[17] R. Asahi, T. Morikawa, H. Irie, T. Ohwaki, *Chem. Rev.* **2014**, 114, 9824-9852.
[18] Y. Ide, N. Inami, H. Hattori, K. Saito, M. Sohmiya, N. Tsunoji, K. Komaguchi, T. Sano, Y. Bando, D. Golberg, Y. Sugahara, *Angew. Chem. Int. Ed.* **2016**, 55, 3600-3605.
[19] C. P. Kumar, N. O. Gopal, T. C. Wang, M. S. Wong, S. C. Ke, *J. Phys. Chem. B* 2006, **110**, 5223-5229.
[20] a) G. Li, N. M. Dimitrijevic, L. Chen, J. M. Nichols, T. Rajh, K. A. Gray, *J. Am. Chem. Soc.* **2008**, 130, 5402-5403; b) S. Maurelli, M. Vishnuvarthan, M. Chiesa, G. Berlier, S. Van Doorslaer, *J. Am. Chem. Soc.* **2011**, 133, 7340-7343.
[21] C. E. Barrera-Diaz, V. Lugo-Lugo, B. Bilyeu, *J. Hazard. Mater.* **2012**, 223-224, 1-12.
[22] L. Pan, J. J. Zou, X. W. Zhang, L. Wang, *J. Am. Chem. Soc.* **2011**, 133, 10000-10002.
[23] Y. N. Liu, C. C. Shen, N. Jiang, Z. W. Zhao, X. Zhou, S. J. Zhao, A.W. Xu, *ACS Catal.* **2017**, 7, 8228-8234.

COMMUNICATION

Band-gap state engineering: band-gap states are introduced to the surface electronic structure of rutile TiO_2 by substitutional doping N for the in-plane O of (110) facet without resorting to the surface disorder. The remarkable capacity of Cr(VI) reduction accentuates the ascendancy of unambiguous adsorption sites and efficient surface charge transfer provided by the active surface heteroatom-sites.

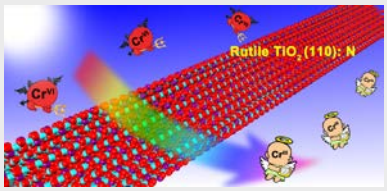

Yaoguang Yu, Xu Yang, Yanling Zhao, Xiangbin Zhang, Liang An, Miaoyan Huang, Gang Chen and Ruiqin Zhang**

Page No. – Page No.

Band-gap state engineering in rutile TiO_2 (110) surface by modulating the active heteroatom